First Principles Search for Multiferroism in $BiCrO_3$

Nicola A. Hill*

Materials Department, University of California, Santa Barbara, California 93106-5050

Pio Bättig and Claude Daul

Department of Chemistry, Université de Fribourg, Pérolles, CH-1700 Fribourg, Switzerland

Received: August 17, 2001; In Final Form: December 18, 2001

We present results of first-principles density functional calculations for the candidate multiferroic magnetoelectric, bismuth chromite. Although little is known experimentally about $BiCrO_3$, its chemical neighbors $BiMnO_3$ and $BiFeO_3$ are known to be ferromagnetic and ferroelectric respectively, with structural distortions driven by the strongly polarizable Bi ions. Our calculations reveal, as expected, a Bi-induced distortion, and an octahedral Cr^{3+} ion which resists off-center displacement. We predict a G-type antiferromagnetic ground state, with an antiferrodistortive or antiferroelectric structural distortion, similar to that seen in $PbZrO_3$.

1. Introduction

Multiferroic magnetoelectrics are materials which are both ferromagnetic and ferroelectric in the same phase.[1] As a result they have a spontaneous magnetization which can be switched by an applied magnetic field, a spontaneous polarization which can be switched by an applied electric field, and often some coupling between the two. Such materials have all the potential applications of both their parent ferroelectric and ferromagnetic materials. In addition, a whole range of new applications can be envisaged.[2] First, the ability to couple either to the electric or the magnetic polarization allows an additional degree of freedom in the device design. Other applications include multiple state memory elements, in which data is stored both in the electric and the magnetic polarizations, or novel memory media which might allow writing of a ferroelectric data bit, and reading of the magnetic field generated by association. Aside from the potential applications, the fundamental physics of multiferroic materials is rich and fascinating.

Very few multiferroic materials exist in nature, or have been synthesized in the laboratory. Earlier work on perovskite structure oxides[3] showed that in general the existence of transition metal d electrons, which are essential for magnetism, reduces the tendency for off-center ferroelectric distortion. Consequently, an additional electronic or structural driving force must be present for ferromagnetism and ferroelectricity to occur simultaneously.

Perovskite structure oxides containing Bi as the large cation are particularly promising candidate multiferroic materials. In fact preliminary experiments on $BiMnO_3$[4] suggest that recent theoretical predictions of ferroelectricity in ferromagnetic $BiMnO_3$ may indeed be correct.[5] The origin of the ferroelectricity is believed to be a relative Bi−O displacement (rather than the displacement of the small cation which is observed in conventional perovskite structure ferroelectrics) resulting from the stereochemical activity of the lone pair on the Bi cation.[6] The $(6s)^2$ electrons, rather than remaining spherical, mix with p states to form a space-filling localized lobe, which in turn pushes away its neighboring atoms causing a structural distortion. The only $BiXO_3$ compound (X = trivalent transition metal) that has been studied experimentally in any detail is $BiFeO_3$. It is known to be ferroelectric below 1110 K, and antiferromagnetic with a Néel temperature of 670 K.[7] It shows the linear magnetoelectric effect, with applied magnetic fields inducing weak ferromagnetism and large increases in electric polarization.[8] Note that the Fe^{3+} ion in $BiFeO_3$ has the d^5 electron configuration, and therefore is not a Jahn−Teller ion.

Little is known about $BiCrO_3$ (in which the formally Cr^{3+} ion has three 3d electrons). A 1968 paper reported it to be antiferromagnetic with a weak ferromagnetic moment below 123 K.[9] The effective Bohr magneton number was found to be close to the spin-only value for Cr^{3+} above 123 K, but to be anomalously large (4.7) below 123 K. These results have not been confirmed. A high-temperature structural phase was reported to be pseudomonoclinic with lattice parameters $a = c = 3.878$ Å, $b = 7.765$ Å, and $\beta = 88.8°$. Superstructure lines were observed, and could be assigned to a unit cell doubled along the *b* direction, with adjacent Bi^{3+} ions shifted in opposite directions. A first-order phase transition with thermal hysteresis was observed at around 400 K, below which the structure was pseudo-triclinic with no superstructure lines. The measured lattice parameters were $a = c = 3.906$ Å, $b = 3.870$ Å, $\alpha = \gamma = 90.5°$, and $\beta = 88.8°$. The most recent experimental work,[10] from 1974, performed differential thermal analysis and ac conductivity measurements. A crystallization temperature of 1201 K and a polymorphic phase transition without temperature hysteresis at 1155 K were observed. The small number of phase transitions and lack of thermal hysteresis in comparison to $BiFeO_3$ were attributed to the very slight distortions of the octahedral environment of Cr^{3+}. There have been no investigations (to our knowledge) of ferroelectricity.

Our theoretical study of $BiCrO_3$ is motivated in part by the well-known resistance of the Cr^{3+} ion to displacement from its centrosymmetric position in an octahedral environment. The Cr^{3+} ion has a d^3 configuration, which means that the t_{2g} shell is completely filled with one electron per orbital. As a result, Cr^{3+} is not a Jahn−Teller ion; instead the d electron charge distribution is spherically symmetric and therefore resistant to

* To whom correspondence should be addressed. Tel: (805) 893-7920. Fax: (805) 893-7221. E-mail: nahill@mrl.ucsb.edu.

10.1021/jp013170m CCC: $22.00
Published on Web 03/09/2002

any off-center displacement. As a result any ferroelectric distortion, if present at all, must arise from the Bi ions. Thus $BiCrO_3$ provides an ideal test case for studying displacement mechanisms for the large cation in perovskite oxides. We hope that our theoretical results will also stimulate experimental interest in this less-well-studied material.

The remainder of this paper is organized as follows: In section 2 we describe the local spin density approximation (LSDA) implementations of density functional theory (DFT) which we use for this study. In section 3 we present results of our calculations for $BiCrO_3$ in an idealized undistorted cubic phase for a variety of magnetic symmetries. We compare our results to earlier calculations for $BiMnO_3$ in order to isolate the role of the transition metal cation from that of the Bi ion. In section 4 we investigate the nature of the structural instabilities in $BiCrO_3$ with particular focus on potential ferroelectric distortions. Our results are summarized in section 5.

2. Computational Technique

The calculations described in this work were performed using plane wave pseudopotential (PWPP)[11] and linearized augmented plane wave (LAPW)[12] implementations of density functional theory[13] within the local spin density approximation (LSDA) and generalized gradient approximation (GGA). Although the accuracy and efficiency of ab initio pseudopotential calculations for magnetic systems is now fairly well established (see, for example, refs 5 and 14−16), a direct comparison with all-electron methods is useful for confirming the validity of both the pseudopotentials and the implementation.

2.1. Technical Details. Pseudopotential calculations of total energy, band structure and response properties were performed on AMD Athlon PCs using the ABINIT[17] and Spinor[18] plane wave pseudopotential codes. We used a high plane wave cut off of 50 hartrees, and a $48 \times 48 \times 48$ sampling grid to represent the density, potential and wave functions. The Perdew−Zunger parametrization[19] of the Ceperley−Alder LSDA exchange correlation potential[20] with the von Barth−Hedin interpolation formula[21] was used. A $4 \times 4 \times 4$ Monkhorst−Pack[22] grid was used for calculations with a simple cubic unit cell. This led to 10 k-points in the irreducible Brillouin zone for the high-symmetry cubic structures, and a correspondingly higher number for the distorted structures with lower symmetry. A variable Gaussian broadening between 1 and 0.002 eV was applied to the k-point sampling to speed convergence for metallic systems. For Cr and O we used standard Troullier−Martins[23] pseudopotentials with local components $l = 0$ and $l = 1$, respectively. Nonlinear core corrections[24] were included in the Cr pseudopotential. For Bi, we constructed a scalar-relativistic Troullier−Martins pseudopotential using the Fritz−Haber Institute fhi98PP program,[25] with the d electrons included in the valence state. Although the 3d electrons lie around 25 eV below the Fermi energy, and show minimal (0.03 eV) dispersion, their omission results in approximately 10% reduction in the lattice constant. All pseudopotentials were put into the usual Kleinman−Bylander form,[26] and the absence of ghost states was confirmed using the ghost theorem of Gonze, Käckell, and Scheffler.[27]

All-electron calculations were performed using the Wien 97.A10 full potential LAPW package[28] on a DEC GS60 workstation and on a Beowulf cluster composed of 23 Pentium III processors. The muffin-tin radius was set to 1.8 Å for all atoms, and a $16 \times 16 \times 16$ k-point mesh was used. The exchange−correlation functional was treated both with the Perdew−Zunger LSDA functional, and the GGA using the Perdew−Burke−Ernzerhof functional.[29] Unless otherwise stated, graphs plotted in this paper show results obtained within the local spin density approximation.

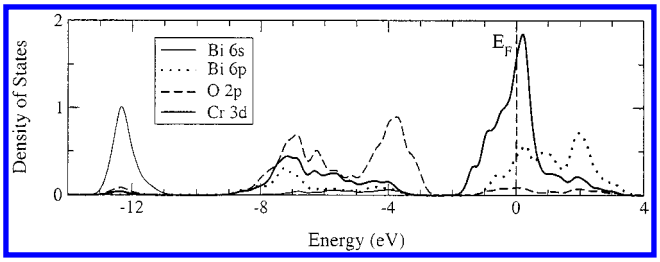

Figure 1. Orbital resolved densities of states for cubic paramagnetic $BiCrO_3$ calculated within the LSDA. The high density of states at the Fermi level indicates that this is an unstable phase.

3. Calculated Electronic Properties of $BiCrO_3$

We begin by calculating the electronic structure of $BiCrO_3$ in the high symmetry cubic phase, without including magnetic effects, then lower the magnetic symmetry to the ferromagnetic, and probable antiferromagnetic phases. Finally, we introduce structural distortions in both paramagnetic and ferromagnetic calculations. This ability to isolate structural and magnetic distortions is unique to computational studies, and allows identification of the essential microscopic interactions which cause the observed macroscopic behavior.

3.1. Cubic Paramagnetic Structures. First, we present results for $BiCrO_3$ in the highest possible symmetry state, that is, the cubic structure, without spin polarization (we call this the paramagnetic (PM) phase). Although this phase is experimentally inaccessible, it provides a useful reference for understanding the spin-polarized structures to be discussed later in this paper. We find a minimum energy lattice constant of 3.87 Å, slightly underestimating the average of the experimental unit cell edge lengths as expected within the local density approximation.

Figure 1 shows the orbital resolved densities of states in the Bi 6s and 6p, oxygen 2p, and Cr 3d states from 14 eV below to 4 eV above the Fermi energy (which is set to zero eV). No other orbitals contribute significantly to the density of states in this region. A sharp peak at −12 eV corresponding to the Bi 6s states is clearly visible. Note that the broad band between −2 and −8 eV, although largely composed of O 2p states, also has significant contribution from the Bi 6p and Cr 3d states. Hybridization between Cr 3d and the surrounding oxygen ligands is expected, and of course leads to the well-known super-exchange interactions in magnetic perovskites.[30] However, the occupied Bi 6p bands are at first sight unexpected. We will see later that these have profound consequences on the structural properties of this material. The density of Cr 3d states at the Fermi level is high, and so, by the usual Stoner argument,[31] this phase should be unstable with respect to spin polarization or structural distortion (or both).

In Figure 2 we compare our calculated band structure of paramagnetic $BiCrO_3$ plotted along the high-symmetry axes of the simple cubic Brillouin zone, to that of $BiMnO_3$ calculated in earlier work.[5] Again the Fermi level is set to 0 eV in both cases. The most striking feature in comparing the band structures of $BiCrO_3$ and $BiMnO_3$ is their similarity. The broad O 2p bands between −2 and −8 eV can be seen to have almost identical structure in both materials, as do the transition metal 3d bands which lie above them, separated by an energy gap. The highlighted lines in the $BiMnO_3$ band structure plot accentuate the upper and lower Mn 3d bands which have a similar form to the corresponding bands in other perovskite structure manga-

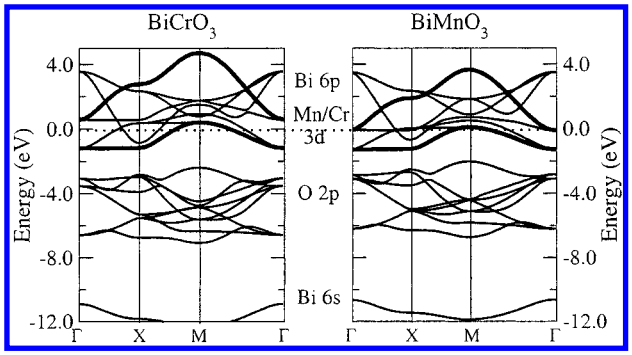

Figure 2. Calculated band structures for cubic paramagnetic $BiCrO_3$ and $BiMnO_3$ along the high-symmetry axes of the Brillouin zone. The highlighted lines in the band structure plots accentuate the upper and lower Cr 3d and Mn 3d bands, which have a similar form to each other and to those of other transition metal perovskites.

nites. Similarly, the highlighted bands in the $BiCrO_3$ band structure accentuate the lower and upper Cr 3d bands. We see that they have a similar form to the Mn 3d bands. In both cases the Bi 6s band lies around 4 eV below the bottom of the O 2p bands, and has significant dispersion, indicative of hybridization with the O 2p bands. In addition, both the Mn 3d bands in $BiMnO_3$ and the Cr 3d bands in $BiCrO_3$ occupy the same energy ranges as their respective Bi 6p orbitals. The most notable difference between the two band structures is the almost rigid shift in energy of the Fermi level relative to the transition metal d bands, resulting from the extra d electron in the formally d^4 Mn^{3+} ion compared with the d^3 Cr^{3+}. The different experimental magnetic orderings occurring in these compounds (FM for $BiMnO_3$ and AFM for $BiCrO_3$) are likely the result of the different numbers of d electrons driving different structural distortions which in turn stabilize different magnetic order.

3.2. Cubic Ferromagnetic Structures. Next, we present the results of calculations in which the high-symmetry cubic structure is retained, but the electrons are allowed to spin polarize. We find that the ferromagnetic structure has a GGA magnetic moment of 2.95 μ_B, which is close to the Hund's rule value of 3 μ_B expected for the d^3 configuration. The slight reduction from the maximum possible magnetization is the result of hybridization between the Cr 3d and O 2p electrons which is seen clearly in the band structure and is discussed below. The LSDA magnetic moment is slightly lower again (2.80 μ_B), reflecting the well-established overestimation of p−d hybridization within the local density approximation.

We find that introduction of spin polarization reduces the energy of $BiCrO_3$ by around 600 meV per formula unit within the LSDA, and around 900 meV within the GGA. The source of the stabilization is apparent in the density of states, shown in Figure 3, which shows a significant reduction at the Fermi level compared with the paramagnetic phase, consistent with the Stoner model. The DOS at E_F is still finite however, and has sizable contributions from both Cr 3d and Bi 6p states. This suggests that either the ferromagnetic phase of $BiCrO_3$ is not the most stable, and that an AFM spin arrangement will further lower the energy of the system, or that the cubic phase is unstable, and a structural distortion will lower the energy. Since Cr^{3+} is a d^3 ion which usually resists distortion from perfect cubic symmetry in an octahedral environment, the latter would indicate unusual behavior driven by the Bi ion. The GGA DOS (not shown) is almost identical to the LSDA DOS, although the lower hybridization leads to very slightly narrower bands. This in turn causes a slightly lower DOS at E_F and an additional stabilization over the non-spin-polarized phase compared to the stabilization calculated in the local density approximation.

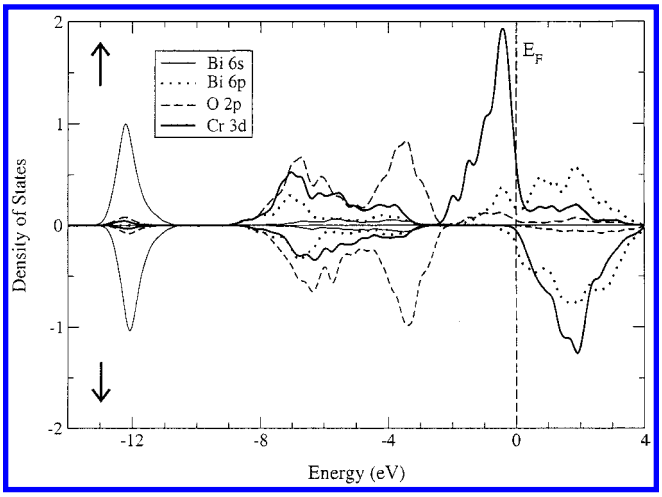

Figure 3. Orbital resolved densities of states for cubic ferromagnetic $BiCrO_3$ calculated within the LSDA. Note that the density of states at the Fermi level is lower than that in the paramagnetic phase.

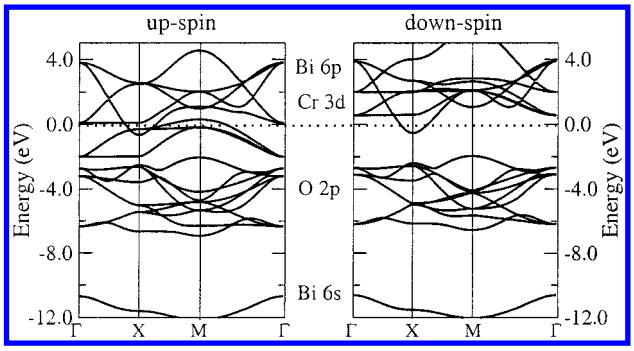

Figure 4. Up- and down-spin LSDA band structures for cubic ferromagnetic $BiCrO_3$ along the high-symmetry axes of the Brillouin zone.

Figure 4 shows the up and down-spin LSDA band structures for $BiCrO_3$ along the high-symmetry axes of the simple cubic Brillouin zone. The first notable point is that the Fermi energy is now very close to a band gap region for the minority carriers, so that the system is almost half-metallic. For the majority carriers, E_F almost divides the t_{2g} and e_g bands, as expected for a formal charge of d^3 in an exchange split system in an octahedral environment. The nonexchange-split Bi 6s, Bi 6p, and O 2p bands are almost identical for up- and down-spin, and are similar to the corresponding bands in the paramagnetic band structure. Thus the effect of the exchange splitting is to introduce an almost rigid shift of the Cr 3d bands, with the up-spin bands moving down in energy relative to the PM phase, and the down-spin bands moving up in energy and becoming unoccupied.

3.3. Antiferromagnetic Structures. Finally, we calculate the total energy of $BiCrO_3$ in both the A-type antiferromagnetic (in which adjacent planes of ferromagnetically aligned Cr^{3+} ions are aligned antiferromagnetically) and G-type antiferromagnetic (in which each Cr^{3+} ion is surrounded by neighbors of the opposite spin) cubic phases. Super-exchange arguments[30] predict that the cubic G-type structure should be the most stable, as is observed in $CaMnO_3$ (in which the Mn^{4+} ion also has the t_{2g}^3 configuration). This is in fact the case, as we see from Table 1 which shows our calculated relative energies for the PM, FM, A-type AFM, and G-type AFM phases.

In fact we find that the energies of both AFM structures are lower than that of the FM phase, although the gain in stability

TABLE 1: Relative Energies of Different Magnetic Phases in Cubic Paramagnetic $BiCrO_3$

	LSDA energy (meV)	GGA energy (meV)
PM	0	0
FM	−603	−925
A-AFM	−656	
G-AFM	−721	−1045

in allowing spin polarization from the paramagnetic phase is much larger than the differences between different magnetic orderings. Note that, as pointed out above, the GGA predicts a larger stabilization on introduction of spin-polarization than the LSDA, since the more realistic slightly narrower GGA bands are closer to having a gap at the Fermi level in the magnetic structures. However the energy difference between the most stable G-type antiferromagnetic structure, and the ferromagnetic phase, is the same in both approximations (120 meV).

In Figure 5 we show the calculated GGA band structure of G-type AFM $BiCrO_3$ plotted along the high-symmetry lines of the larger fcc Brillouin zone (containing two formula units per unit cell). We choose to plot the GGA in this case to emphasize that imposition of G-type AFM symmetry is insufficient to open a gap in the cubic structural phase (A-type AFM $BiCrO_3$ is quite similar and therefore not shown here) even in calculations that go beyond the LSDA. The broad band crossing the Fermi energy is composed largely of Bi 6p character.

There is one notable change from the ferromagnetic band structure, however, and that is the complete spin-splitting of the majority Cr d states. The Fermi level now lies at the upper edge of the majority t_{2g} states which are now fully occupied, and the majority e_g states are now completely unoccupied. All minority d states are unoccupied. There is no significant change in crystal field splitting (around 2.5 eV) or exchange splitting (slightly less than 4 eV) compared with the ferromagnetic phase, but the majority t_{2g} band is slightly narrower and therefore does not intersect with the Fermi energy. The fact that only the Bi 6p band intersects the Fermi energy suggests that a gap can be opened by a structural distortion that involves rehybridization of the Bi 6p states alone.

4. Ferroelectric Distortions?

Our calculations of different magnetic orientations indicate that $BiCrO_3$ can only become insulating by undergoing a structural distortion, since the Bi 6p states intersect the Fermi energy whatever the magnetic ordering in the cubic phase. In this section we calculate the structural instabilities inherent in the cubic phase, to determine the structural ground state.

The cubic perovskite structure has five atoms per unit cell, which results in 15 phonon branches, 3 acoustical, and 12 optical. At the Γ point all phonons are 3-fold degenerate, so there is one acoustical phonon frequency (which is zero, corresponding to a translation), and four optical frequencies. We are interested in the optical phonons which have negative eigenvalues, indicating lattice instabilities. Note that since $BiCrO_3$ is metallic in its cubic phases, we are unable to obtain an optical dielectric constant from calculations for the prototypical cubic structure, and consequently, the calculated LO−TO splitting is zero.

We obtain the full phonon band structure for the paramagnetic structure, by fitting the interatomic force constants[32] to the phonon eigenvalues and eigenvectors calculated at the high-symmetry points of the Brillouin zone. It is interesting to note that the self-force constants, which specify the force on an atom when it is displaced by unit displacement, are all positive. This indicates that $BiCrO_3$ is stable against displacement of an *isolated* atom, and collective atom displacements are required to stabilize the distorted structure. In addition, note that the repulsive force created on the Bi ion when it is displaced is rather small, as expected for such a highly polarizable ion. In contrast the Cr self-force constant is large, indicating a reluctance of the Cr^{3+} ion to move off-center.

The calculated phonon band structure is shown in Figure 6. Phonons plotted with negative frequencies are in fact imaginary and indicative of lattice instabilities. Note the strongly unstable phonon branch which has been observed previously in calculations for many other ferroelectric perovskites.[32] The most strongly unstable branches are dominated by bismuth and oxygen contributions, with no significant chromium character. This is reminiscent of the behavior of $PbZrO_3$, in which a strongly unstable mode results from Pb−O interactions, but quite different to the case of $BaTiO_3$ in which Ti and O contribute most strongly to the unstable modes. The strongly unstable modes at R and M correspond to rotations of the oxygen octahedra, while the less unstable modes at X and M consist of the Bi ion moving in opposition to one of the oxygen ions. The eigenvector of the Γ point mode corresponds to a displacement pattern in which the Bi ion moves in the opposite direction to all the other ions, as shown in Figure 7. This mode results in formation of a dipole moment within the unit cell, and is a ferroelectric distortion. The displacement amplitudes are +0.536 (Bi), −0.122 (Cr), −0.196 (axial O), and −0.574 (equatorial O). Note that this mode has a similar frequency to that of the corresponding mode in PM $BiMnO_3$, indicating that, at least in the paramagnetic phase, the instability is driven by the stereochemical activity of the Bi ion, and is insensitive to the nature of the small cation.

Finally we calculated the changes in local density of states and charge densities with the Γ point phonon mode frozen in as a static distortion. The magnitude of the distortion was chosen to be rather large, with the Bi ion moving by 5% along the *z* axis and the other displacements scaled proportionally, to emphasize any changes. We found the new LDOSs to be very similar to those of the undistorted structure, and therefore they are not re-plotted here. The only notable change is a shift down in energy of the upper part of the O 2p band (and corresponding decrease in O 2p bandwidth). This is notable for two reasons. First, in classic ferroelectric perovskites such as $BaTiO_3$, the driving force for the off-center distortion is a strong sigma- and pi- bonding interaction between the Ti 3d and O 2p orbitals which results in marked changes in the local densities of states of these orbitals.[33] Clearly the lone pair formation driving the off-center distortion in this case is quite a different mechanism. Second, the only observed change is a lowering of the O 2p and *not* the Bi 2p energy levels. This suggests that, in contrast to the classical lone pair picture, the localized lone pair in the distorted structure is not composed only of the expected Bi 6s and 6p states, but also has some contribution from the 2p states on the oxygen ligands. This has recently been observed in a number of related materials.[6,34]

The lone pair localization can be seen clearly in the changes in *charge density* between the undistorted cubic structure and the structure with the Γ point phonon mode frozen in as a static distortion. Figures 8 and 9 show contour plots of the charge density in the (010) plane of the cubic structure and the distorted structure, respectively. In the ideal cubic structure this plane has a Bi ion at each unit cell corner and an oxygen ion in the center of the face. We see that the charge density around the Bi ions is quite spherical, and the Bi−O hybridization is

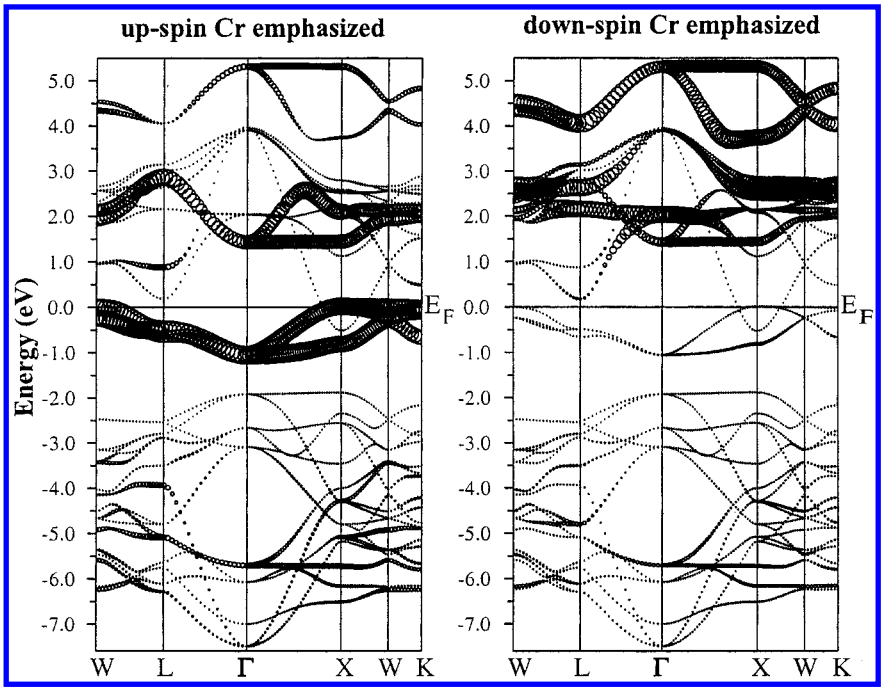

Figure 5. Band structure of A-type antiferromagnetic $BiCrO_3$, plotted along the high-symmetry axes of the face centered cubic Brillouin zone.

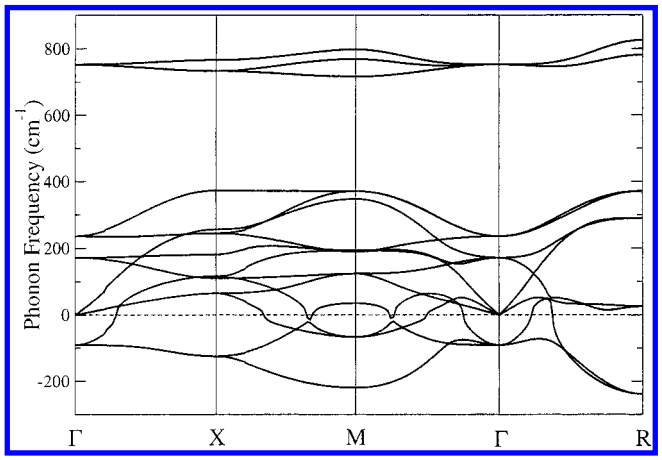

Figure 6. Full phonon band structure of $BiCrO_3$.

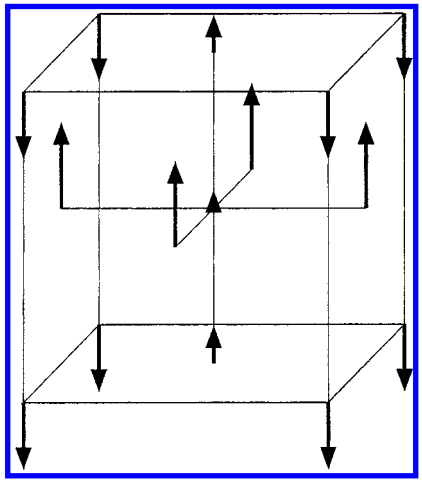

Figure 7. Eigenvectors of the ferroelectric unstable Γ point phonon mode in $BiCrO_3$. The Cr ion is at the center of the unit cell surrounded by an octahedron of oxygens, with the Bi ions at the unit cell corners.

minimal. The distortion consists of the Bi ion displaced along the *z* axis (vertically upward in this view) by 5% of the lattice constant, with the other ions moved vertically downward

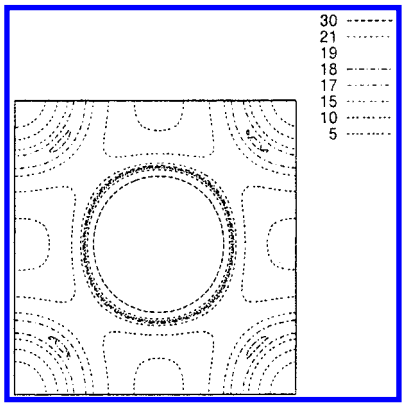

Figure 8. Charge density plots in the (010) plane of cubic $BiCrO_3$. The Bi ions are at the corners with an oxygen ion in the center.

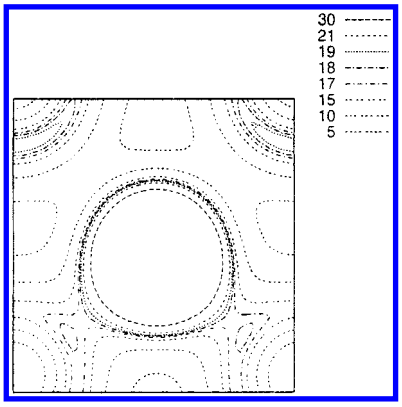

Figure 9. Charge density plots in the (010) plane of distorted $BiCrO_3$ with the Γ point ferroelectric distortion frozen in.

proportionally. In the lower half of the picture, where the Bi and oxygen ions have moved closer together, a build-up of charge density in the Bi−oxygen bond can be seen clearly, indicating an increase in Bi−O hybridization. In the upper corners of the picture, where the Bi ion has moved up out of the range of the plot, the charge density localizes into a lobe shape corresponding to lone pair localization.

5. Summary

In summary, we have shown that $BiCrO_3$, like its counterparts $BiMnO_3$ and $BiFeO_3$, is unstable in the ideal cubic perovskite phase, with a structural instability driven by the stereochemical activity of the Bi lone pair. However the formally trivalent Cr ion, with its filled t_{2g}^3 shell, prefers to retain its ideal octahedral environment. Our calculations predict an A-type antiferromagnetic ground state, consistent with a simple super-exchange picture, and a distorted structure that is antiferroelectric and/or antiferrodistortive. Therefore $BiCrO_3$ is unlikely to be a technologically relevant multiferroic material. However it is an ideal model material for elucidating the role of the A cation in driving structural phase transitions in perovskite structure ferroelectrics. Therefore further experimental study is to be encouraged.

Acknowledgment. Nicola Hill acknowledges financial support from the National Science Foundation's Division of Materials Research, Grant DMR-9973076, and thanks Umesh Waghmare, Karin Rabe, and Ram Seshadri for useful discussions. Claude Daul acknowledges the UCSB Materials Research Laboratory for their hospitality during his sabbatical leave, and the Swiss National Science Foundation for financial support. Pio Bättig would like to thank Fabio Mariotti for the introduction to Wien97 and for the provided support throughout the work. This work made use of MRL Central Facilities supported by the National Science Foundation under Award DMR00-80034.

References and Notes

(1) Schmid, H. *Ferroelectrics* **1994**, *162*, 317.
(2) Wood, V. E.; Austin, A. E. *Magnetoelectric Interaction Phenomena in Crystals*; Freeman, A. J., Schmid, H., Eds.; Gordon and Breach: Langhorne, PA, 1975.
(3) Hill, N. A. *J. Phys. Chem. B.* **2000**, *104*, 6694.
(4) Santos, A. M.; Raju, A. R.; Parashar, S.; Cheetham, A. K.; Rao, C. N. R. Private communication.
(5) Hill, N. A.; Rabe, K. M. *Phys. Rev. B.* **1999**, *59*, 8759.
(6) Seshadri, R.; Hill, N. A. *Chem. Mater.* **2001**, *13*, 2892.
(7) Sosnowska, I.; et al. *J. Phys. C* **1982**, *15*, 4835.
(8) Popov, Y. F.; et al. *JETP Lett.* **1993**, *57*, 69.
(9) Sugawara, F.; Ida, S.; Syono, Y.; Akimoto, S. *J. Phys. Soc. Jpn.* **1968**, *25*, 1553. Tomashpol'skii, Y. Y.; Venetsev, Yu. N. *Sov. Phys. Cryst.* **1972**, *16*, 905.
(10) Reznitskii, L. A. *Inorg. Mater.* **1974**, 993−994 (June), translated from *Izvestiya Akademii Nauk SSSR, Neorganische Materialy* **1974**, *10* 1156.
(11) Yin, M. T.; Cohen, M. L. *Phys. Rev. B* **1982**, *26*, 5668.
(12) Jepsen, O.; Andersen, O. K. *Phys. Rev. B* **1975**, *12*, 3060;
(13) Hohenberg, H.; Kohn, W. *Phys. Rev.* **1964**, *136*, 864; Kohn, W.; Sham, L. J. *Phys. Rev.* **1965**, *140*, 1133.
(14) Sasaki, T.; Rappe, A. M.; Louie, S. G. *Phys. Rev. B* **1995**, *52*, 12760.
(15) Cho, J.-H.; Kang, M.-H. *Phys. Rev. B* **1995**, *52*, 9159.
(16) Lewis, S. P.; Allen, P. B.; Sasaki, T. *Phys. Rev. B* **1997**, *55*, 10253.
(17) The ABINIT code is a common project of the Universite Catholique de Louvain, Corning Incorporated, and other contributors (WWW: http://www.pcpm.ucl.ac.be/abinit.
(18) The Spinor code is publicly available under the GNU General Public License at http://www.mrl.ucsb.edu/ theurich/Spinor/.
(19) Perdew, J. P.; Zunger, A. *Phys. Rev. B* **1981**, *23*, 5048.
(20) Ceperley, D. M.; Alder, B. J. *Phys. Rev. Lett.* **1980**, *45*, 566.
(21) von Barth, U.; Hedin, L. *J. Phys. C* **1972**, *5*, 1629.
(22) Monkhorst, H. J.; Pack, J. D. *Phys. Rev. B* **1976**, *13*, 5188.
(23) Troullier, N.; Martins, J. L. *Phys. Rev. B* **1991**, *43*, 1993.
(24) Louie, S. G.; Froyen, S.; Cohen, M. L. *Phys. Rev. B* **1982**, *26*, 1738.
(25) http://www.FHI−Berlin.MPG.DE/th/fhi98md/fhi98PP. Fuchs, M.; Scheffler, M. *Comput. Phys. Commun.* **1999**, *119*, 67.
(26) Kleinman, L.; Bylander, D. M. *Phys. Rev. Lett.* **1982**, *48*, 1425.
(27) Gonze, X.; Käckell, P.; Scheffler, M. *Phys. Rev. B* **1990**, *41*, 12264.
(28) Blaha, P.; Schwarz, K.; Luitz, J. *WIEN97, A Full Potential Linearized Augmented Plane Wave Package for Calculating Crystal Properties*; Karlheinz Schwarz, T. U. Wien: Vienna, 1997. ISBN 3-9501031-0-4.
(29) Perdew, J. P.; Burke, K.; Ernzerhof, M. *Phys. Rev. Lett.* **1996**, *77*, 3865.
(30) Goodenough, J. B. *Phys. Rev.* **1955**, *100*, 564.
(31) Stoner, E. C. *Proc. R. Soc.* **1938**, *165*, 372.
(32) Ghosez, Ph.; Cockayne, E.; Waghmare, U. V.; Rabe, K. M. *Phys. Rev. B* **1999**, *60*, 836.
(33) Filippetti, A.; Hill, N. A. *Phys. Rev. B.* **2002**. Submitted for publication.
(34) Watson, G. W.; Parker, S. C. *J. Phys. Chem. B* **1999**, *103*, 1258. Watson, G. W.; Parker, S. C.; Kresse, G. *Phys. Rev. B.* **1999**, *59*, 8481.